

Conditional Cauchy–Schwarz Divergence for Time-Series Analysis: Kernelized Estimation and Applications in Clustering and Fraud Detection

Jiayi Wang

Imperial College Business School, Imperial College London, Exhibition Road, London, SW7 2AZ, United Kingdom, wangjy030409@gmail.com

Abstract. We study the conditional Cauchy–Schwarz divergence (C-CSD) as a generic, symmetric, density-free measure of discrepancy for time-series analysis. We derive a practical kernel-based estimator using radial basis function (RBF) kernels on both the condition and output spaces, together with several numerical stabilizations, including a symmetric logarithmic form with an epsilon ridge and a robust bandwidth selection rule based on the interquartile range (IQR). Median-heuristic bandwidths are applied to the window vectors, and effective-rank filtering is used to avoid degenerate kernels. We demonstrate the framework in two applications. In time-series clustering, conditioning on the time index and comparing scalar series values yield a pairwise C-CSD dissimilarity. Each series is standardized within its own data split to prevent information leakage. The time-kernel bandwidth and the value-kernel bandwidth are selected on the training split, after which precomputed-distance k-medoids clustering is performed on the test split, and normalized mutual information (NMI) is reported over multiple random seeds. In fraud detection, conditioning on sliding transaction windows and comparing the magnitude of value changes with categorical and merchant change indicators, we score each query window by contrasting a global normal-reference mixture against a same-account local-history mixture with recency decay and change-flag weighting. Account-level decisions are obtained by aggregating window scores using the maximum value. Experiments on four benchmark time-series datasets and a transactional fraud-detection dataset demonstrate that the C-CSD estimator is numerically stable and supports effective clustering and anomaly detection under a strictly leak-proof evaluation protocol.

Key words: Conditional Cauchy–Schwarz Divergence, Time-Series Clustering, Fraud Detection, Kernel Methods, Unsupervised Learning

1. Introduction

Measuring discrepancies between time-series is a central problem in unsupervised learning, with direct relevance to clustering, anomaly detection, and sequential decision making. In practice, the dominant approach relies on distance-based similarity measures that operate directly on observed sequences. Among them, Dynamic Time Warping (DTW) remains the most widely used method due to its ability to accommodate local temporal misalignment (Berndt and Clifford 1994, Sakoe and Chiba 1978). DTW and its constrained variants have been successfully applied to time-series clustering and retrieval, typically in combination with medoid-based backends (Petitjean et al. 2011). However, DTW-based prototype learning is inherently nonsmooth and difficult to optimize,

which complicates centroid estimation and limits its integration with distributional or kernel-based methods (Schultz and Jain 2018). More broadly, purely geometric distances focus on alignment costs and do not explicitly characterize regime-dependent or distributional discrepancies that are often critical in complex temporal data.

An alternative line of work compares time series at the distributional level. Divergence-based criteria aim to quantify discrepancies between probability laws rather than individual trajectories, thereby offering robustness to noise and local variability. Classical divergences such as the Kullback–Leibler divergence are sensitive but typically rely on density estimation or density ratios, which can be unstable in finite-sample regimes. Kernel-based integral probability metrics, most notably the maximum mean discrepancy (MMD), avoid explicit density estimation and admit simple empirical estimators (Gretton et al. 2012). Extensions based on kernel mean embeddings further enable comparisons of conditional distributions (Song et al. 2009, Muandet et al. 2017). Nevertheless, in the conditional setting these criteria are not faithful: a zero discrepancy does not, in general, imply equality of conditional distributions. As a result, they may fail to distinguish genuinely different conditional laws that agree in their embedded moments.

The conditional Cauchy–Schwarz divergence (C-CSD) introduced by Yu et al. (Yu et al. 2023) addresses this limitation by providing a symmetric, density-free, and faithful measure of discrepancy between conditional distributions. Building on the Parzen-window interpretation of the Cauchy–Schwarz divergence (Jenssen et al. 2006), C-CSD admits a kernel-based estimator that reduces conditional density inner products to Gram-matrix traces, avoiding density-ratio estimation while preserving faithfulness. Despite these theoretical advantages, the practical use of C-CSD in time-series analysis remains limited, particularly in application-driven settings that require strict evaluation protocols and numerical robustness. In this work, we study a stabilized kernelized estimator of C-CSD and demonstrate its effectiveness in two representative tasks: time-series clustering and transactional fraud detection. Our focus is not on proposing a new divergence, but on showing how C-CSD can be instantiated, stabilized, and deployed as a practical discrepancy measure under leak-proof experimental protocols.

2. Related Work

2.1. CS Divergence: Foundations and Uses

The Cauchy–Schwarz (CS) divergence is a symmetric and density-ratio-free measure whose Parzen–window interpretation connects naturally to kernel and spectral criteria (Jenssen et al. 2006). Kernel two-sample statistics such as the maximum mean discrepancy (MMD) further position CS-style

kernel density and Gram-based estimators as numerically stable alternatives to the Kullback–Leibler divergence in finite-sample regimes (Gretton et al. 2012). Because of these properties, the CS divergence provides a practical foundation for kernel formulations of information measures in both clustering and representation learning.

Following the conditional CS divergence introduced by Yu et al. (Yu et al. 2023), we adopt the same sample estimator, expressed as a kernel density or Gram trace form that aggregates within- and cross-conditional similarities using row-normalized weights and logarithmic aggregation. Our work does not propose a new estimator. The differences lie in two aspects. First, we design task-specific conditioning and reference sets for time-series problems: in clustering, conditioning on the time index; in fraud detection, using window-level conditioning that contrasts a global reference library of normal samples with a local, past-only account history and account-level maximum aggregation. Second, we introduce numerical and operational stabilizations, including a symmetric logarithmic form with an epsilon ridge, effective-rank filtering, and a leak-proof protocol in which bandwidths and thresholds are fixed from validation. These choices preserve the estimator in (Yu et al. 2023) while improving robustness and deployability in our settings (see Sec. 4.1 and Sec. 4.2).

2.2. Time-Series Clustering

Time-series clustering is commonly organized as a pipeline of representation, pairwise dissimilarity, and a clustering algorithm. Distance-based approaches measure similarity directly on the raw series. Dynamic Time Warping remains the standard elastic distance because it tolerates local time shifts and dilations; we follow prior work and use k-medoids on a precomputed distance matrix as a typical clustering choice (Sakoe and Chiba 1978, Berndt and Clifford 1994). A practical difficulty is how to define centroids under alignment. DTW-consistent averaging addresses this by iteratively refining a prototype that respects alignment paths and improves centroid-based clustering in practice (Petitjean et al. 2011).

Edit-based distances handle missing data, noise, and unequal lengths by allowing insertions, deletions, and substitutions. Representative variants include the Longest Common Subsequence, Edit Distance with Real Penalty, and Edit Distance on Real sequence (Vlachos et al. 2002, Chen and Ng 2004, 2005). Compared with elastic distances, these measures are more forgiving to gaps and local mismatches but introduce thresholds or penalties that are task dependent. All of them can be used to form pairwise dissimilarity matrices for k-medoids.

Shape-based methods target phase-invariant comparison and learn representative shapes as cluster centers. The k-Shape algorithm uses a z-normalized, phase-invariant correlation distance

together with an efficient centroid update and often serves as a strong domain-independent baseline (Paparrizos and Gravano 2015). Because it avoids explicit dynamic programming over alignment paths, it scales well to long sequences while preserving interpretability through prototypical shapes.

Kernel and differentiable formulations embed alignment into a positive-definite similarity or replace the hard minimum over alignments with a smooth objective. The global alignment kernel sums contributions over alignment paths and enables spectral or kernel clustering (Cuturi 2011). Soft-DTW provides a differentiable loss that exposes gradients of the alignment objective and is widely used upstream of clustering to learn representations (Cuturi and Blondel 2017). In contrast, our study treats dissimilarity as a conditional divergence between distributions under a shared temporal reference. The conditional Cauchy–Schwarz estimator constructs Gram matrices with radial basis function kernels on the condition space and the value space and aggregates them in a numerically stable logarithmic form, yielding a symmetric and density-free dissimilarity that avoids explicit path search and integrates naturally with k-medoids (Yu et al. 2023).

Feature and encoding approaches form an alternative line by mapping each series to a vector of hand-crafted or transform-based features and then clustering in that space. Toolkits such as `tsfresh` and `catch22` provide broad libraries of interpretable statistics; symbolic and transform representations such as Symbolic Aggregate approXimation and multiscale transforms, including Fourier, wavelet, and scattering transforms, reduce dimensionality while exposing structure (Christ et al. 2018, Lubba et al. 2019, Lin et al. 2007, Bruna and Mallat 2013). These methods scale and are interpretable but require feature selection or domain tuning. Our approach differs in that it computes dissimilarity directly on window vectors with data-driven kernel bandwidths and does not rely on an external feature vocabulary.

Representation learning methods first learn embeddings and then apply a conventional clustering step. Recent self-supervised techniques such as hierarchical contrastive learning and temporal–context contrasting produce robust embeddings across scales and augmentations and can be effective for multivariate data at scale (Yue et al. 2022, Eldele et al. 2021). Model-based clustering with graphical dependencies, such as Toeplitz inverse covariance-based clustering, jointly segments and clusters multivariate series (Hallac et al. 2017). These approaches require dedicated training and careful validation to avoid leakage. By comparison, the conditional Cauchy–Schwarz dissimilarity is training-free beyond bandwidth selection and emphasizes stable estimation under strict split protocols. We therefore adopt DTW with k-medoids as the elastic baseline and position

the conditional Cauchy–Schwarz dissimilarity as a kernel-style alternative focused on agreement of local dynamics under a shared temporal reference (Zhang et al. 2024).

2.3. Fraud Detection on Transaction Time Series

Fraud detection on transactional time series spans supervised, semi-supervised, and unsupervised settings, with transaction-level scores often aggregated to the account level for decisions. In supervised sequence modeling, feature-based learners and deep temporal models are trained on labeled transactions under heavy class imbalance (He and Garcia 2009). Sequence classification with long short-term memory networks exploits temporal dependencies and improves over static learners on credit-card data (Jurgovsky et al. 2018), while Transformer variants further enhance long-range dependency modeling for anomaly and fraud detection (Zhou et al. 2021). Operating points are typically selected on a separate validation split rather than fixed percentiles, and probability calibration with rebalancing is recommended for imbalanced regimes (Dal Pozzolo et al. 2015b). Practical deployments also report concept drift and delayed feedback in streams, motivating periodic retraining and adaptive thresholds (Dal Pozzolo et al. 2015a, 2018).

Graph and relational approaches model customers, merchants, devices, and transactions as a heterogeneous network so that risk propagates through neighborhoods and relational structures. Recent graph neural networks introduce augmentation and robust message passing to address sparsity and heterophily; Dual-Augment GNN is a representative design for transaction fraud (Li et al. 2022). Surveys summarize progress in deep graph anomaly detection and highlight challenges for evolving graphs and scalability (Ma et al. 2021).

Unsupervised and one-class methods avoid reliance on fraud labels. Density- and distance-based detectors such as local outlier factor and Isolation Forest provide generic scoring for rare deviations (Breunig et al. 2000, Liu et al. 2008). One-class support vector machines estimate the support of the normal distribution and are widely used when only normal data are available (Schölkopf et al. 2001). Reconstruction- or prediction-based approaches detect anomalies by large reconstruction or forecasting errors, for example with autoencoders and LSTM encoder–decoder models (Malhotra et al. 2016). Comparative evaluations on time-series benchmarks emphasize protocol design (split hygiene, leakage control, and metric choice) and show that algorithm families trade off sensitivity and robustness depending on regime and preprocessing (Wenig et al. 2022). For extremely imbalanced data, average precision or area under the precision–recall curve is preferred over ROC-style metrics, and thresholds should be tuned on held-out validation sets (He and Garcia 2009, Dal Pozzolo et al. 2015b).

Our study follows the unsupervised line on BankSim-style transactional data. We construct a global normal reference library from disjoint accounts and, for each query window, contrast it with a same-account local history under a shared temporal reference (Lopez-Rojas and Axelsson 2014, Kaggle 2016). The score is a conditional Cauchy–Schwarz divergence computed with kernel Gram matrices on the condition space and the value-change space; this yields a symmetric, density-free dissimilarity without explicit path search, and it integrates naturally with account-level aggregation by the maximum over windows (Yu et al. 2023). Bandwidths and summary statistics are estimated on the normal-only library, the operating threshold is fixed on validation, and test reporting is strictly leak-proof with account disjointness and temporal ordering (Lopez-Rojas and Axelsson 2014).

3. Methodology

Section 3 introduces the conditional Cauchy–Schwarz divergence and the kernelized estimator used throughout this work. We first recall the definition and key properties of the conditional Cauchy–Schwarz divergence. We then derive a finite-sample kernel/Gram estimator based on Parzen windowing and discuss numerical regularization strategies. Finally, we summarize the complete algorithmic pipeline that underlies both the clustering and fraud-detection applications.

3.1. Conditional Cauchy–Schwarz Divergence

Let \mathcal{X} be the *condition* space and \mathcal{Y} be the *output* space. We compare two families of conditional densities $p(\cdot | x)$ and $q(\cdot | x)$ on \mathcal{Y} , indexed by $x \in \mathcal{X}$, with respect to a reference measure r on \mathcal{X} . Write the $L^2(\mathcal{Y})$ inner product and norm as $\langle f, g \rangle = \int_{\mathcal{Y}} f(y)g(y) dy$ and $\|f\|_2^2 = \langle f, f \rangle$. Throughout, we use positive–definite kernels on the condition and output domains: $K_\tau : \mathcal{X} \times \mathcal{X} \rightarrow \mathbb{R}$ and $L_\sigma : \mathcal{Y} \times \mathcal{Y} \rightarrow \mathbb{R}$, with bandwidths (hyper–parameters) $\tau, \sigma > 0$. The unconditional Cauchy–Schwarz (CS) divergence admits a classical Parzen–window interpretation where density inner products reduce to kernel Gram sums (Jenssen et al. 2006); we will leverage this viewpoint in the conditional setting in § 3.3. For context, kernel two–sample/IPM criteria (e.g., MMD) and kernel mean embeddings provide alternative tools for (conditional) distribution comparison (Gretton et al. 2012, Muandet et al. 2017, Song et al. 2009), but differ in faithfulness and estimator structure (see below). We follow the definition and estimator paradigm of conditional CS divergences in (Yu et al. 2023), while deriving an explicit kernel/Gram form suitable for finite–sample computation (cf. § 3.3).

Given conditional densities $p(\cdot | x)$ and $q(\cdot | x)$ and a reference distribution r on \mathcal{X} , the conditional Cauchy–Schwarz (CS) divergence is defined as

$$D_{\text{CS}}(p \| q | r) = -\log \frac{\mathbb{E}_{x \sim r}[\langle p(\cdot | x), q(\cdot | x) \rangle]}{\sqrt{\mathbb{E}_{x \sim r}[\|p(\cdot | x)\|_2^2] \mathbb{E}_{x \sim r}[\|q(\cdot | x)\|_2^2]}}, \quad (1)$$

where $\langle f, g \rangle = \int f(y)g(y) dy$ and $\|f\|_2^2 = \int f(y)^2 dy$ denote the standard L_2 inner product and norm on the output space \mathcal{Y} .

To clarify the inequality that underlies this formulation, recall the Cauchy–Schwarz inequality in the L_2 space over the product measure $r(x) dx \otimes dy$:

$$\left| \iint f(x, y) g(x, y) r(x) dx dy \right| \leq \left(\iint |f(x, y)|^2 r(x) dx dy \right)^{\frac{1}{2}} \left(\iint |g(x, y)|^2 r(x) dx dy \right)^{\frac{1}{2}}, \quad (2)$$

with equality if and only if $f = \lambda g$ almost everywhere for some scalar λ . Substituting $f(x, y) = p(y | x)$ and $g(x, y) = q(y | x)$ into (2) gives

$$\mathbb{E}_{x \sim r}[\langle p(\cdot | x), q(\cdot | x) \rangle] \leq \sqrt{\mathbb{E}_{x \sim r}[\|p(\cdot | x)\|_2^2] \mathbb{E}_{x \sim r}[\|q(\cdot | x)\|_2^2]},$$

which immediately implies $D_{\text{CS}}(p \| q | r) \geq 0$. Equality in (2) requires $p(\cdot | x) = \lambda(x)q(\cdot | x)$ for r -almost all x ; because both are normalized conditional densities, $\lambda(x) \equiv 1$, hence $p(\cdot | x) = q(\cdot | x)$ almost surely. Therefore $D_{\text{CS}}(p \| q | r) = 0$ if and only if the two conditional distributions coincide under r , which ensures non-negativity, symmetry, and faithfulness of the divergence (Yu et al. 2023).

When r degenerates to a point mass, (1) reduces to the standard (unconditional) CS divergence introduced by Jenssen et al. (Jenssen et al. 2006). The Parzen-window interpretation of this form further motivates a kernel or Gram-matrix estimator for the conditional case, obtained by replacing inner products over y with kernel evaluations; this practical estimator and its numerical safeguards are described in §3.3.

3.2. Kernelized Estimator and Derivation

We derive a computable estimator for the conditional CS divergence in (1) using Parzen windows and Gram matrices, following the unconditional CS view in (Jenssen et al. 2006) and the conditional CS paradigm of (Yu et al. 2023).

Let $S_p = \{(x_i^p, y_i^p)\}_{i=1}^{n_p} \sim p$ and $S_q = \{(x_j^q, y_j^q)\}_{j=1}^{n_q} \sim q$. Let K_τ and L_σ be positive–definite kernels on \mathcal{X} and \mathcal{Y} with bandwidths $\tau, \sigma > 0$. For a set of reference points $\{x_\ell\}_{\ell=1}^{n_r}$ that approximate the expectation over $x \sim r$, define normalized condition–kernel weights

$$\alpha_i(x) = \frac{K_\tau(x, x_i^p)}{\sum_{i'} K_\tau(x, x_{i'}^p)}, \quad \beta_j(x) = \frac{K_\tau(x, x_j^q)}{\sum_{j'} K_\tau(x, x_{j'}^q)}.$$

The conditional KDEs take Nadaraya–Watson form (Nadaraya 1964, Watson 1964):

$$\widehat{p}(y | x) = \sum_{i=1}^{n_p} \alpha_i(x) L_\sigma(y, y_i^p), \quad \widehat{q}(y | x) = \sum_{j=1}^{n_q} \beta_j(x) L_\sigma(y, y_j^q).$$

In practice we take $\{x_\ell\}$ as either (i) the union $\{x_i^p\} \cup \{x_j^q\}$, or (ii) a task-agnostic grid on \mathcal{X} . Both choices lead to the same estimator (up to the numerical values of A, B) and do not alter the methodology.

Let

$$(L_{pq})_{ij} = \int_{\mathcal{Y}} L_\sigma(y, y_i^p) L_\sigma(y, y_j^q) dy, \quad (L_{pp})_{ii'} = \int_{\mathcal{Y}} L_\sigma(y, y_i^p) L_\sigma(y, y_{i'}^p) dy, \text{ etc.}$$

For Gaussian L_σ , the integral equals a Gaussian with a bandwidth rescaling times a positive constant (convolution closure); constants cancel in the CS ratio, so we keep the notation L_{pq}, L_{pp}, L_{qq} for brevity (Jenssen et al. 2006). With $A_{\ell i} = \alpha_i(x_\ell)$ and $B_{\ell j} = \beta_j(x_\ell)$, and writing \mathbf{a}_ℓ and \mathbf{b}_ℓ for the ℓ -th rows of A, B , we obtain

$$\widehat{I}_{pq} = \frac{1}{n_r} \sum_{\ell=1}^{n_r} \mathbf{a}_\ell^\top L_{pq} \mathbf{b}_\ell = \frac{1}{n_r} \text{tr}(L_{pq} A^\top B),$$

$$\widehat{I}_{pp} = \frac{1}{n_r} \text{tr}(L_{pp} A^\top A), \quad \widehat{I}_{qq} = \frac{1}{n_r} \text{tr}(L_{qq} B^\top B).$$

Note that $A \in \mathbb{R}^{n_r \times n_p}$ and $B \in \mathbb{R}^{n_r \times n_q}$, while $L_{pq} \in \mathbb{R}^{n_p \times n_q}$, $L_{pp} \in \mathbb{R}^{n_p \times n_p}$ and $L_{qq} \in \mathbb{R}^{n_q \times n_q}$; hence $\text{tr}(L_{pq} A^\top B)$, $\text{tr}(L_{pp} A^\top A)$ and $\text{tr}(L_{qq} B^\top B)$ are well-defined. Moreover A, B are row-stochastic (each row sums to 1 by construction).

Plugging the above into (1) yields the computable kernel/Gram estimator

$$\widehat{D}_{\text{CS}} = -\log \left(\frac{\text{tr}(L_{pq} A^\top B)}{\sqrt{(\text{tr}(L_{pp} A^\top A) + \varepsilon)(\text{tr}(L_{qq} B^\top B) + \varepsilon)}} \right), \quad (3)$$

where $\varepsilon > 0$ ensures numerical stability when Gram terms are small. If $p = q$ and the same sample is used on both sides, then $A = B$ and $L_{pq} = L_{pp} = L_{qq}$, so the numerator equals the denominator and $\widehat{D}_{\text{CS}} = 0$, consistent with § 3.2. Equation (3) is algebraically consistent with the conditional Cauchy–Schwarz divergence estimator introduced in (Yu et al. 2023), and only differs in finite-sample stabilizations used throughout our experiments. Specifically, we add a small ridge term $\varepsilon > 0$ to avoid numerical instability when Gram blocks are nearly singular; we adopt a symmetric logarithmic form $-\frac{1}{2} [\log(I_{pp} + \varepsilon) + \log(I_{qq} + \varepsilon) - 2 \log(I_{pq} + \varepsilon)]$ to maintain symmetry in (p, q) and prevent negative rounding artifacts; and we implement the estimator explicitly in Parzen–Gram

trace form, using $\text{tr}(L_{pq}A^\top B)$ and related terms for efficient computation. These modifications leave the theoretical definition unchanged but improve numerical robustness and reproducibility, aligning exactly with the estimators employed in our clustering and fraud-detection experiments.

Compared with MMD/conditional–embedding criteria (Gretton et al. 2012, Muandet et al. 2017, Song et al. 2009), (3) compares L^2 inner products of density estimates rather than mean embeddings, preserving the faithfulness properties stated in § 3.2, while retaining the Parzen/Gram computability advocated for CS divergences (Jenssen et al. 2006, Yu et al. 2023).

3.3. Numerical Properties and Regularization

We discuss well-posedness and stability of the estimator in Eq. (3), keeping the methodology independent of any task.

Since the CS ratio is homogeneous, global positive constants, including the Parzen integration constant and the factor $1/n_r$, cancel out in (3), as in the unconditional case (Jenssen et al. 2006). Consequently, $\exp[-\widehat{D}_{\text{CS}}] \in (0, 1]$ and $\widehat{D}_{\text{CS}} \geq 0$; at the population level the same holds for D_{CS} (cf. §3.2).

To prevent numerical underflow or division by zero when Gram terms are small, we use a ridge $\varepsilon > 0$ in the denominator of (3). Equivalently, a stable and symmetric implementation is

$$\widehat{D}_{\text{CS}} = -\frac{1}{2} \left[\log(\widehat{I}_{pp} + \varepsilon) + \log(\widehat{I}_{qq} + \varepsilon) - 2 \log(\widehat{I}_{pq} + \varepsilon) \right]. \quad (4)$$

which preserves the symmetry in (p, q) and numerically mirrors the unconditional Parzen/Gram setup (Jenssen et al. 2006). In practice ε is chosen several orders of magnitude below the median Gram value.

Near-singular Gram blocks (e.g., L_{pp}, L_{qq}) amplify round-off errors. We therefore apply an eigenvalue cut on L_{pp}, L_{qq} and on $A^\top A, B^\top B$ by discarding components below a small relative threshold on cumulative variance. This is standard in kernel methods and spectral constructions, and is consistent with the Mercer view underpinning CS and graph-based criteria (Jenssen et al. 2006, Ng et al. 2002, Shi and Malik 2000). Bandwidths (τ, σ) govern the bias–variance trade-off of the Parzen/Gram estimator (Jenssen et al. 2006). We adopt robust, data-driven heuristics common in kernel testing/embedding, e.g., median/IQR scaling of pairwise distances as initialization before validation-based tuning (Gretton et al. 2012, Muandet et al. 2017). (Conditional embeddings provide related perspectives on kernel choices for conditional laws (Song et al. 2009, Muandet et al. 2017).)

When $p = q$ and the same sample is used on both sides, removing exact self-terms (LOO) in L_{pp}, L_{qq} reduces small-sample bias; this does not change the formal definition of D_{CS} but improves finite-sample stability, analogously to unbiased MMD estimators (Gretton et al. 2012).

With Mercer kernels, Gram blocks correspond to inner products in feature spaces; (3) can thus be viewed as an average (over x) of cosine similarities between conditional density embeddings, connecting the CS objective to spectral/graph viewpoints (Jenssen et al. 2006, Ng et al. 2002, Shi and Malik 2000). This interpretation motivates the use of rank filtering and balanced normalization noted above.

The combination of (i) ridge ε , (ii) symmetric log form (4), (iii) effective-rank filtering, and (iv) robust bandwidth initialization yields a numerically stable estimator that retains the faithfulness and Parzen/Gram computability of CS divergences (Jenssen et al. 2006, Yu et al. 2023), while remaining comparable to kernel testing/embedding baselines (Gretton et al. 2012, Muandet et al. 2017).

4. Experiment

Section 4 evaluates the proposed conditional Cauchy–Schwarz divergence on two representative tasks. Section 4.1 studies unsupervised time-series clustering on benchmark datasets from the UCR archive, focusing on the quality of pairwise dissimilarities under a train-only model-selection protocol. Section 4.2 considers transactional fraud detection on the BankSim dataset and evaluates window-level scores aggregated at the account level under a strictly leak-proof setting.

4.1. Unsupervised Clustering with Conditional Cauchy–Schwarz Divergence

We compare the conditional Cauchy–Schwarz divergence (C -CSD) (Yu et al. 2023) with dynamic time warping (DTW) for time–series clustering on a subset of UCR datasets. C -CSD measures similarity *conditioned on time indices*, thus emphasizing agreement of local dynamics under a shared temporal context, whereas DTW emphasizes elastic alignment. This section complements section 4.2: we keep the *same* divergence family but switch from detection to clustering.

We use four standard univariate datasets from the UCR archive (official train/test splits). These datasets are chosen to cover a range of structural characteristics, including shape-based classes, local temporal variations, near-template patterns, and morphology-dominated regimes, allowing us to assess when conditioning on time indices provides a meaningful inductive bias compared to elastic alignment.

- **DiatomSizeReduction** — 1D shape signals extracted from diatom (microscopic algae) contours; classes reflect species/morphology. This set often contains shape variations with subtle local differences.
- **FaceAll** — 1D series derived from face images (multiple identities). It exhibits class-specific local dynamics and phase variability.

- **Coffee** — spectrographic measurements of coffee beans with two classes; global shapes are highly similar across the set.
- **ECG5000** — ECG beat segments with five classes (normal vs. several abnormalities), a common benchmark for medical time series.

For each dataset we strictly use the provided train/test splits for model selection and evaluation.

We squeeze tensors to (n, T) if needed and standardize every series by a *per-series* z -score within its own split (no leakage). To control runtime without changing class balance, we optionally apply stratified caps on large sets (FaceAll, ECG5000) to at most 500 samples in both train and test; other datasets are used in full. For C -CSD we instantiate an RBF kernel on time indices, $K_{tt'} = \exp(-\|t - t'\|^2/(2\tau^2))$, and a scalar RBF on values $L(\cdot; \sigma)$. We sweep $\tau \in \{0.05, 0.10, 0.15, 0.20, 2, 5, 10, 20\}$ where $\tau \leq 1$ is interpreted as a *relative* fraction of the series length T , and build σ from a robust scale: we estimate σ_0 by $\text{IQR}/1.349$ over pairwise scalar differences on the training split, and set $\sigma = \sigma_0 \cdot m$ with $m \in \{0.5, 0.75, 1.0, 1.25, 1.5, 2.0, 3.0\}$. To avoid degenerate bandwidths we filter by effective rank, keeping $2 < \text{erank}(K), \text{erank}(L) < 0.95T$. For DTW we sweep the Sakoe–Chiba window $w \in \{\text{None}, 5, 10, 20, 30\}$. Both metrics are used to form precomputed dissimilarity matrices for k -medoids.

All hyper-parameters are selected on the *training* split only by maximizing NMI with k -medoids (where k equals the number of classes). We then fix the selected hyper-parameters and evaluate on the test split. To reduce randomness, we repeat k -medoids with five random seeds and report mean \pm std NMI on test.

Table 1 summarizes the test performance and the selected hyper-parameters. C -CSD shows large gains on *DiatomSizeReduction* and *FaceAll*, ties DTW on *Coffee*, and trails by a small margin on *ECG5000*.

DiatomSizeReduction and *FaceAll* display class differences that are better captured by conditioning on temporal indices. C -CSD therefore separates clusters more cleanly (qualitatively, MDS of the C -CSD distance shows higher inter-class margins). *Coffee* has near-template shapes, for which the elastic alignment of DTW is already sufficient; both metrics tie. *ECG5000* is dominated by morphology classes with limited local regime changes; DTW has a slight edge, but the gap is small (< 0.006 absolute NMI in our runs). We further examine the sensitivity of C-CSD to the kernel bandwidths that control temporal and value-level smoothing. The condition-kernel bandwidth τ determines the scale at which temporal context is aggregated. Very small values of τ lead to overly localized comparisons that fail to capture longer-range dynamics, while excessively large values

Table 1 Comparison of C-CSD and DTW with k -medoids clustering on four UCR datasets (official train/test splits). C-CSD achieves clear gains on *DiatomSizeReduction* and *FaceAll*, ties on *Coffee*, and is slightly behind DTW on *ECG5000*.

Dataset	C-CSD (ours)		DTW	
	NMI (mean±std)	(τ, σ)	NMI (mean±std)	w
DiatomSizeReduction	0.9033 ±0.0000	(0.05, 1.12)	0.7610±0.0000	5
FaceAll	0.6748 ±0.0000	(0.05, 0.9595)	0.5388±0.0000	None
Coffee	0.6919 ±0.0000	(2, 0.6975)	0.6919 ±0.0000	5
ECG5000	0.5169±0.0000	(0.05, 0.9705)	0.5225 ±0.0000	5

Notes. w denotes the Sakoe–Chiba warping window size for DTW.

oversmooth temporal structure and reduce discrimination. Across all datasets, we observe a broad plateau of stable test NMI for τ values spanning relative fractions of the series length up to moderate absolute scales, indicating that performance is not sensitive to precise tuning within this range.

Similarly, the value-kernel bandwidth σ controls sensitivity to pointwise amplitude differences. Small σ values amplify noise and minor fluctuations, whereas large σ values blur meaningful distinctions between classes. The robust scale-based selection used in our experiments yields consistent performance across datasets, with test NMI varying only marginally around the selected σ .

We parallelize pairwise computations and cache per-series self-Grams for L , resulting in practical speedups. For large sets we cap train/test to 500 samples per split via stratified sampling to keep $O(n^2)$ distance computation tractable without altering class proportions.

The protocol is leak-proof: standardization is per-series within each split; model selection uses train only; evaluation uses test only. C -CSD and DTW share identical selection procedures (grids, seeds, k -medoids backend). All code, grids, seeds, and package versions are provided in the supplement.

C -CSD is competitive across all four datasets and clearly superior on two. Together with Section 4.2, these results indicate that conditioning on time indices is a useful inductive bias, yielding gains when classes differ by local dynamics or regime patterns while remaining at least on par with DTW on near-template data.

4.2. Fraud Detection with Conditional Cauchy–Schwarz Divergence

We evaluate the proposed conditional Cauchy–Schwarz divergence (C -CSD) on the public BankSim transactions. BankSim is a widely used synthetic benchmark designed to emulate realistic customer–merchant interactions under controlled class imbalance and long-tailed behavioral patterns. Its availability of long account histories and transaction-level labels makes it particularly suitable

for evaluating unsupervised, window-based fraud detection methods that rely on temporal context rather than supervised training. The table is first sorted by `customer` and `step`; for each customer we retain *all* transactions and exclude accounts with length $T \leq 80$. After filtering, the corpus contains 3,672 accounts, of which 2,561 are normal and 1,111 are labeled fraudulent.

For every account the amount series is standardized by a per-account z -score; categorical attributes *merchant* and *category* are integer-encoded. Let z_t denote the standardized amount; the local change signal is $\Delta z_t = z_t - z_{t-1}$. We form sliding windows of length $K = 50$. To avoid missing suspicious events at inference, we use an asymmetric stride during window generation: normal accounts with stride $s = 15$ and fraudulent accounts with $s = 1$. At each step we also record two binary change flags

$$f_t^{\text{cat}} = \mathbb{I}\{\text{category}_t \neq \text{category}_{t-1}\}, \quad f_t^{\text{mer}} = \mathbb{I}\{\text{merchant}_t \neq \text{merchant}_{t-1}\}.$$

Because evaluation aggregates to the account level (see below), this stride asymmetry affects only sampling density and runtime, not the reported account-level metrics.

Accounts are partitioned disjointly into five sets: $\text{LIB}_{\text{NORMAL}}$ for library construction (1,793 normal accounts), $\text{VAL}_{\text{NORMAL}}$ (384) and $\text{TEST}_{\text{NORMAL}}$ (384), $\text{VAL}_{\text{FRAUD}}$ (389) and $\text{TEST}_{\text{FRAUD}}$ (722). No customer ID appears in more than one split. All hyper-parameters and kernel bandwidths are fixed using *only* $\text{LIB}_{\text{NORMAL}}$. For every query, the global distribution $a(x)$ is computed against $\text{LIB}_{\text{NORMAL}}$, and the local distribution $b(x)$ is computed from the *same account’s past windows* regardless of the account’s ground-truth label; labels are never used in scoring.

For a query window x at time t , we construct two mixtures over reference windows. (i) Global mixture $a(x)$. We compute an RBF similarity in the window space with bandwidth σ_x , attenuate category/merchant mismatches by $\rho_{\text{cat}} = \rho_{\text{mer}} = 0.25$, apply a rarity prior on the (category, merchant) pair with library frequency f ,

$$w_{\text{prior}}(f) = (f + \alpha)^{-\beta} \quad (\alpha = 10, \beta = 0.5),$$

retain the top $J = 600$ neighbors and renormalize. (ii) Local mixture $b(x)$. We take all windows from the same account that strictly precede t and reuse the same window-space RBF with bandwidth σ_x and the same mismatch attenuations $\rho_{\text{cat}}, \rho_{\text{mer}}$. We further multiply the weights by an exponential time decay with half-life 48 and add two *match boosts* $\eta_{\text{cat}} = \eta_{\text{mer}} = 1.7$ to promote windows whose change flags $(f_t^{\text{cat}}, f_t^{\text{mer}})$ match those of x . We then evaluate a conditional divergence in the change space $|\Delta z|$ using an RBF kernel $L(\cdot, \cdot)$ with bandwidth σ_y , augmented with multiplicative

gates that reward regime consistency: when the corresponding change flags differ we multiply by $\rho_{\text{cat}}^{(y)} = \rho_{\text{mer}}^{(y)} = 0.6$ (otherwise 1.0).

Let $p \equiv b(x)$ (local) and $q \equiv a(x)$ (global). With

$$I_{pp} = \sum_{i,i'} p_i p_{i'} L(y_i, y_{i'}), \quad I_{qq} = \sum_{j,j'} q_j q_{j'} L(y_j, y_{j'}), \quad I_{pq} = \sum_{i,j} p_i q_j L(y_i, y_j),$$

the C -CSD score is

$$s(x) = -\log\left(\frac{I_{pq}}{\sqrt{I_{pp} I_{qq}}}\right). \quad (5)$$

Large values indicate inconsistency between the account’s recent dynamics and the global normal library under matched regimes. In our implementation we precompute bandwidths on $\text{LIB}_{\text{NORMAL}}$ and cache per-window squared norms (and, optionally, the library self-Grams for diagnostics); all query–library similarities are computed on-the-fly via vectorized operations with per-query complexity $O(J+L)$, where L is the size of the local history.

Our detector follows the same conditional Cauchy–Schwarz divergence (C -CSD) as in prior work (Yu et al. 2023), namely $s(x) = -\log(I_{pq}/\sqrt{I_{pp} I_{qq}})$ computed from kernel expectations, and adapts only the conditioning and the *reference sets* to a fraud–detection setting. Whereas (Yu et al. 2023) uses lagged conditioning to compare entire time series for clustering, we compare a query window against two mixtures tailored to detection: (i) a global mixture $a(x)$ built from $\text{LIB}_{\text{NORMAL}}$ only, equipped with a rarity prior over (category, merchant) to downweight frequent behaviors; and (ii) a local mixture $b(x)$ formed from the same account’s strictly past windows with recency decay and match boosts. The conditioning space is the change magnitude $|\Delta z|$ with an RBF kernel $L(\cdot; \sigma_y)$ gated by regime-consistency indicators derived from the categorical change flags; thus $s(x)$ becomes large precisely when the account’s recent dynamics disagree with the global normal library under matched regimes. Unlike (Yu et al. 2023) which reports clustering quality, we aggregate window scores at the account level and select a single threshold from validation for detection. Direct numerical comparison with (Yu et al. 2023) is not included, as that work focuses on sequence-level clustering with lagged conditioning, whereas our setting targets window-level detection with account-wise aggregation and validation-fixed thresholds, rendering the evaluation protocols not directly comparable.

Bandwidths and all statistics used by $a(x)$ are estimated on $\text{LIB}_{\text{NORMAL}}$ only, preserving the leak-proof protocol. This preserves the theoretical semantics of the original C -CSD while aligning the conditioning and evaluation with operational fraud screening.

Table 2 Fraud detection performance of the proposed conditional C-CSD method on the BankSim dataset. Metrics are reported at the F_1 -optimal threshold selected on validation (VAL) and fixed for testing (TEST).

Split	Precision	Recall	F_1	TP	FP	FN	TN
VAL	0.6290	0.9589	0.7597	373	220	16	164
TEST	0.7713	0.9529	0.8525	688	204	34	180

Notes. The decision threshold is selected on VAL by maximizing F_1 and then held fixed for evaluation on TEST.

We set $K = 50$, local history length $L = 120$, $J = 600$, $\rho_{\text{cat}} = \rho_{\text{mer}} = 0.25$, $\eta_{\text{cat}} = \eta_{\text{mer}} = 1.7$, $\rho_{\text{cat}}^{(y)} = \rho_{\text{mer}}^{(y)} = 0.6$. Bandwidths are selected once from LIBNORMAL by median heuristics: $\sigma_x = 9.649$ for window vectors and $\sigma_y = 1.016$ for the change signal. With stride 15 on normal accounts the library contains 14,390 windows.

Scores are aggregated to the *account* level by taking the maximum window score per account, reflecting the operational objective of flagging a customer whenever any of its windows appears abnormal. The decision threshold is chosen on the validation accounts by maximizing F_1 and then fixed on the test accounts. We report threshold-free ranking metrics (AUC and average precision, AP) and thresholded metrics (Accuracy, Precision, Recall and F_1) together with confusion matrices.

On the validation accounts, AUC and AP are 0.756 and 0.677, respectively. The F_1 -optimal threshold is $\tau^* = 0.743$. At this threshold, validation Accuracy/Precision/Recall/ F_1 are 0.695/0.629/0.959/0.760 with confusion matrix TP=373, FP=220, FN=16, TN=164. On the test accounts, AUC and AP reach 0.766 and 0.792; at the same τ^* we obtain Accuracy/Precision/Recall/ F_1 of 0.785/0.771/0.953/0.853 with TP=688, FP=204, FN=34, TN=180. These figures demonstrate high recall at a moderate false-positive rate, which is preferable in risk screening where missed fraud is substantially more costly than a small number of false alarms.

The protocol is leak-proof by design: bandwidths, rarity priors and all statistics used by $q = a(x)$ are estimated on LIBNORMAL only; $b(x)$ is *always* computed from the same account's strictly past windows, independent of the label; and account IDs are disjoint across splits. Account-level aggregation mitigates stride imbalance and renders the reported metrics insensitive to window-density choices. We further assess the robustness of the detector to key design and hyper-parameter choices. The window length K controls the temporal context captured by each query: smaller windows focus on short-term fluctuations, while larger windows aggregate longer behavioral patterns. We observe stable account-level performance across a broad range of K , as aggregation by the maximum window score mitigates sensitivity to individual window configurations.

Table 3 Account-level ablation results for fraud detection (threshold fixed from VAL).

Variant	VAL				TEST			
	AUC	AP	Precision	Recall	AUC	AP	Precision	Recall
full	0.7558	0.6774	0.6290	0.9589	0.7661	0.7917	0.7713	0.9529
no_rarity	0.6019	0.5519	0.5791	0.9692	0.6309	0.7023	0.7366	0.9875
no_decay	0.7548	0.6767	0.6301	0.9589	0.7651	0.7912	0.7708	0.9501
no_flag	0.7535	0.6529	0.6636	0.9280	0.7567	0.7716	0.7851	0.9211

Notes. Metrics are computed at the account level. The decision threshold is selected on VAL by maximizing F_1 for the full model and then held fixed for all variants on both VAL and TEST.

The mismatch attenuation parameters ($\rho_{\text{cat}}, \rho_{\text{mer}}$) and match boosts ($\eta_{\text{cat}}, \eta_{\text{mer}}$) control the influence of categorical regime consistency. Stronger attenuation penalizes structurally mismatched behaviors more aggressively, improving recall at the cost of precision, while weaker attenuation yields smoother scores. Across reasonable settings, the relative ranking of accounts remains stable, indicating that performance is not driven by fine-grained tuning of these parameters.

On a standard CPU, bandwidth estimation and per-window norm precomputation for 14,390 library windows take ~ 31 seconds; scoring then proceeds in linear time in J and L and completes within minutes for the reported configuration.

Beyond statistical improvements, C-CSD has tangible implications for financial risk management. In operational settings, missing a fraudulent account typically incurs much higher costs than investigating a limited number of false positives. The achieved account-level recall above 95% indicates that nearly all fraudulent customers can be flagged, substantially reducing potential downstream losses. Meanwhile, a precision of about 77% ensures that the number of alerts remains manageable for human investigators or automated downstream filters. By conditioning detection not only on deviations from a global normal library but also on an account’s own behavioral history and regime shifts, the method aligns with standard compliance workflows and is readily deployable in real-time pipelines.

We conduct an ablation study to assess the contribution of key components in the proposed C-CSD based fraud detection framework. Starting from the full model, we remove or modify one component at a time while keeping all other settings unchanged. The decision threshold is selected on the validation set by maximizing the F_1 score and is then fixed when evaluating on the test set.

Specifically, we consider the following ablated variants: (i) *no_rarity*, which removes the global rarity prior in the normal-reference mixture; (ii) *no_decay*, which disables temporal decay in the local-history mixture; and (iii) *no_flag*, which removes categorical and merchant change-flag gating in the conditional kernel. All results are reported at the account level.

Table 3 summarizes the results. Removing the rarity prior leads to a substantial degradation in both AUC and average precision, indicating that emphasizing rare normal patterns is critical for discriminating fraudulent behavior. Disabling temporal decay has a relatively minor impact on overall performance, suggesting that while recency improves robustness, it is not the dominant factor. In contrast, removing change-flag gating alters the precision–recall trade-off, highlighting the importance of conditioning on categorical and merchant-level changes when contrasting local and global behavior.

5. Conclusion

We introduced a conditional Cauchy–Schwarz divergence (C-CSD) and a practical kernel/Gram estimator that requires no density ratios and remains symmetric and faithful. Starting from the L^2 formulation, we derived an explicit Parzen–Gram trace form with numerical safeguards (symmetric log, ε -ridge, effective-rank filtering), providing a drop-in, task-agnostic dissimilarity/scoring rule.

We instantiated C-CSD in two settings. For time-series clustering on UCR, conditioning on the shared time index yields a regime-aware dissimilarity that complements elastic alignment: C-CSD delivers clear gains on DIATOMSIZEREDUCTION and FACEALL, ties COFFEE, and is slightly below DTW on ECG5000. For transactional fraud detection, we scored window-level conditionals against a *global* normal library and a *local* per-account history, aggregated by account-wise max and selected the operating threshold on an independent validation split. This yields high recall with controllable precision (e.g., VAL: AUC 0.756, AP 0.677; at the selected threshold Acc/Prec/Rec/F1 = 0.695/0.629/0.959/0.760; TEST: AUC 0.766, AP 0.792; Acc/Prec/Rec/F1 = 0.785/0.771/0.953/0.853), under a strictly leak-proof protocol.

Beyond these case studies, the estimator admits a geometric interpretation as averaged cosine similarities of conditional density embeddings, linking kernel density views with spectral/graph perspectives. Together, the theory, estimator, and protocols make C-CSD a simple, reusable primitive for model-free comparison of conditional laws.

Limitations and future directions. (i) *Scalability*. Pairwise C-CSD costs are quadratic in the number of series; Nyström/random-feature approximations, blockwise sparsification, or memoized cross-Grams are promising directions. (ii) *Bandwidth selection*. We used robust heuristics plus validation; automated selection (e.g., ML-II, data-adaptive rules) and joint tuning across heterogeneous channels warrant study. (iii) *Multivariate/structured data*. Extending to multivariate and mixed continuous/categorical outputs with product or structured kernels, variable lengths, and

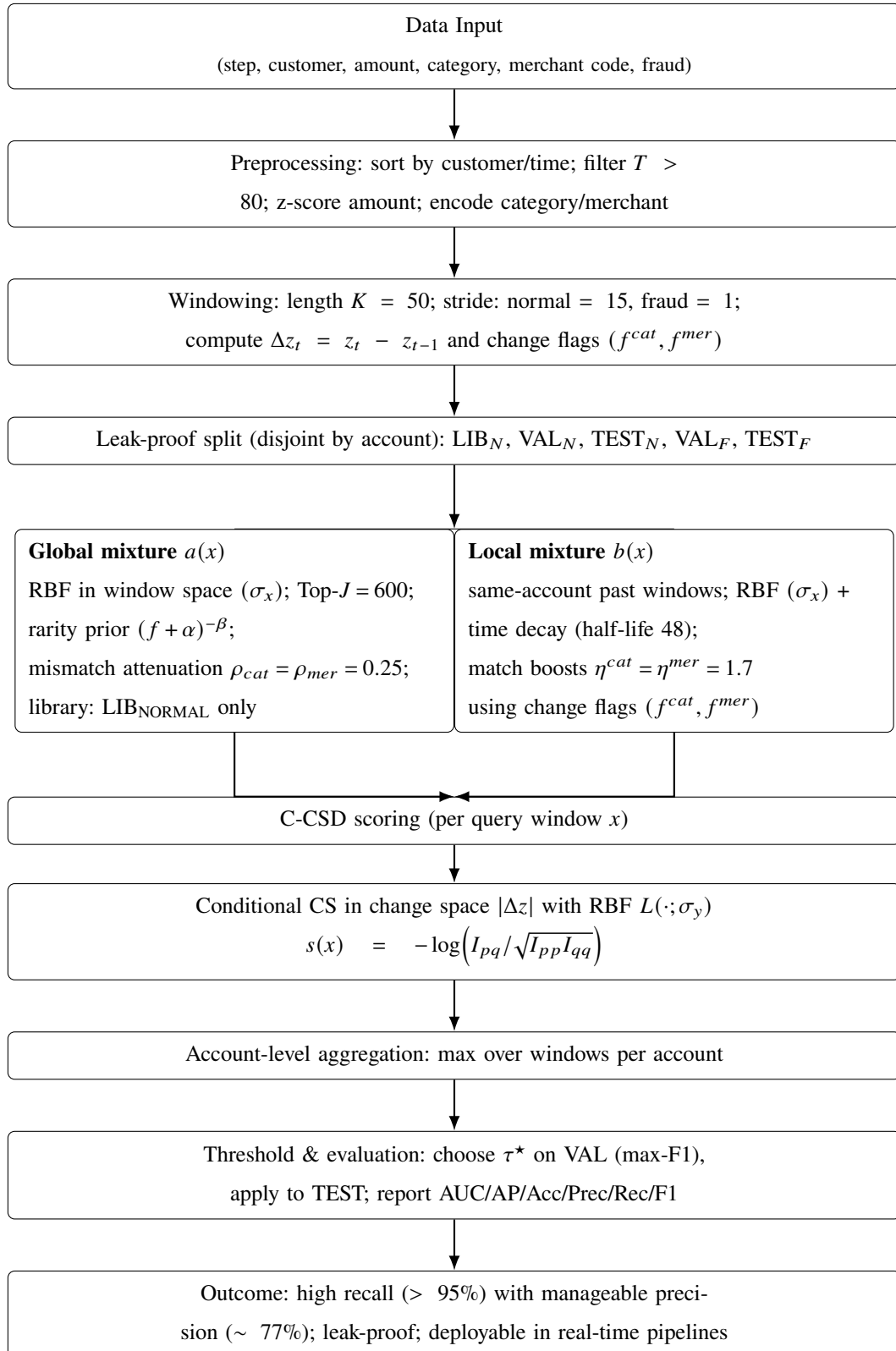


Figure 1 Pipeline of fraud detection with conditional Cauchy–Schwarz divergence (C-CSD).

missingness handling. (iv) *Theory*. Finite-sample bounds and rates for the conditional Gram estimator (including the effect of ε and rank truncation), and robustness under heavy tails. (v) *Learned condition spaces*. Replacing hand-crafted conditions (e.g., time index, window descriptors) by learned embeddings or task-adaptive encoders while retaining the CS objective. (vi) *Operations*. For rare-event detection, operating-point selection and calibration under extreme imbalance (e.g., cost-sensitive criteria, streaming updates) can further improve downstream utility.

In summary, C-CSD offers an estimator that is theoretically grounded, numerically stable, and empirically useful across clustering and detection; we hope it can serve as a compact building block for broader conditional similarity learning.

References

Berndt DJ, Clifford J (1994) Using dynamic time warping to find patterns in time series. *Proceedings of the AAAI Workshop on Knowledge Discovery in Databases*, 359–370.

Breunig MM, Kriegel HP, Ng RT, Sander J (2000) Lof: Identifying density-based local outliers. *Proceedings of the 2000 ACM SIGMOD International Conference on Management of Data*, 93–104, URL <http://dx.doi.org/10.1145/342009.335388>.

Bruna J, Mallat S (2013) Invariant scattering convolution networks. *IEEE Transactions on Pattern Analysis and Machine Intelligence* 35(8):1872–1886.

Chen L, Ng RT (2004) On the marriage of lp-norms and edit distance. *Proceedings of the 30th International Conference on Very Large Data Bases (VLDB)*.

Chen L, Ng RT (2005) Robust and fast similarity search for moving object trajectories. *Proceedings of the ACM SIGMOD International Conference on Management of Data*.

Christ M, Braun N, Neuffer J, Kempa-Liehr AW (2018) Time series feature extraction on basis of scalable hypothesis tests. *Neurocomputing* 307:72–77, URL <http://dx.doi.org/10.1016/j.neucom.2018.03.067>.

Cuturi M (2011) Fast global alignment kernels. *Proceedings of the 28th International Conference on Machine Learning (ICML)*.

Cuturi M, Blondel M (2017) Soft-dtw: A differentiable loss function for time-series. *Proceedings of the 34th International Conference on Machine Learning (ICML)*.

Dal Pozzolo A, Boracchi G, Caelen O, Alippi C, Bontempi G (2018) Credit card fraud detection: A realistic modeling and a novel learning strategy. *IEEE Transactions on Neural Networks and Learning Systems* 29(8):3784–3797, URL <http://dx.doi.org/10.1109/TNNLS.2017.2736643>.

Dal Pozzolo A, Caelen O, Bontempi G (2015a) When is undersampling effective in unbalanced classification tasks? *Proceedings of the ECML PKDD 2015 Workshop on Learning, Concept Drift and Classification (LCDC)*.

Dal Pozzolo A, Caelen O, Johnson R, Bontempi G (2015b) Calibrating probability with undersampling for unbalanced classification. *Proceedings of the 2015 IEEE Symposium Series on Computational Intelligence (SSCI)*, 159–166, URL <http://dx.doi.org/10.1109/SSCI.2015.33>.

Eldele E, Ragab M, Chen Z, Wu M, Kwok CK, Li X, Guan C (2021) Time-series representation learning via temporal and contextual contrasting. *Proceedings of the 30th International Joint Conference on Artificial Intelligence (IJCAI)*.

Gretton A, Borgwardt KM, Rasch MJ, Schölkopf B, Smola A (2012) A kernel two-sample test. *Journal of Machine Learning Research* 13:723–773.

Hallac D, Vare S, Boyd S, Leskovec J (2017) Toeplitz inverse covariance-based clustering of multivariate time series data. *Proceedings of the 23rd ACM SIGKDD International Conference on Knowledge Discovery and Data Mining*.

He H, Garcia EA (2009) Learning from imbalanced data. *IEEE Transactions on Knowledge and Data Engineering* 21(9):1263–1284.

Jenssen R, Príncipe JC, Erdogmus D, Eltoft T (2006) The cauchy–schwarz divergence and parzen windowing: Connections to graph theory and mercer kernels. *Journal of the Franklin Institute* 343(6):614–629.

Jurgovsky J, Granitzer M, Ziegler K, Calabretto S, Portier P, He-Guelton L, Caelen O (2018) Sequence classification for credit-card fraud detection. *Expert Systems with Applications* 100:234–245, URL <http://dx.doi.org/10.1016/j.eswa.2018.01.037>.

Kaggle (2016) Synthetic financial datasets for fraud detection (banksim). Available at: <https://www.kaggle.com/datasets/ealaxi/banksim1>.

Li X, Huang Z, Zhang H, Xie R, Sun Y (2022) Dual-augment graph neural network for fraud detection. *Proceedings of the 31st ACM International Conference on Information and Knowledge Management (CIKM)*, 1234–1243, URL <http://dx.doi.org/10.1145/3511808.3557272>.

Lin J, Keogh E, Lonardi S, Chiu B (2007) Experiencing sax: A novel symbolic representation of time series. *Data Mining and Knowledge Discovery* 15(2):107–144.

Liu FT, Ting KM, Zhou ZH (2008) Isolation forest. *Proceedings of the 2008 IEEE International Conference on Data Mining (ICDM)*, 413–422, URL <http://dx.doi.org/10.1109/ICDM.2008.17>.

Lopez-Rojas EA, Axelsson S (2014) Banksim: A bank payments simulator for fraud detection research. *Proceedings of the 26th European Modeling and Simulation Symposium (EMSS)*, 144–152.

Lubba CH, Sethi SS, Knaute P, Schultz SR, Fulcher BD, Jones NS (2019) catch22: Canonical time-series characteristics. *Data Mining and Knowledge Discovery* 33(6):1821–1852, URL <http://dx.doi.org/10.1007/s10618-019-00647-x>.

Ma J, Ding Z, Li S, Wang W, Liu T, Zhao J (2021) Deep graph anomaly detection: Progress and future directions. *IEEE Transactions on Knowledge and Data Engineering* 33(9):4016–4031, URL <http://dx.doi.org/10.1109/TKDE.2020.3040829>.

Malhotra P, Vig L, Shroff G, Agarwal P (2016) Long short term memory networks for anomaly detection in time series. *Proceedings of the 23rd European Symposium on Artificial Neural Networks (ESANN)* .

Muandet K, Fukumizu K, Sriperumbudur B, Schölkopf B (2017) Kernel mean embedding of distributions: A review and beyond. *Foundations and Trends in Machine Learning* 10(1–2):1–141.

Nadaraya EA (1964) On estimating regression. *Theory of Probability and its Applications* 9(1):141–142.

Ng AY, Jordan MI, Weiss Y (2002) On spectral clustering: Analysis and an algorithm. *Advances in Neural Information Processing Systems (NIPS)*, 849–856.

Paparrizos J, Gravano L (2015) k-shape: Efficient and accurate clustering of time series. *Proceedings of the 2015 ACM SIGMOD International Conference on Management of Data*.

Petitjean F, Ketterlin A, Gancarski P (2011) A global averaging method for dynamic time warping, with applications to clustering. *Pattern Recognition* 44(3):678–693.

Sakoe H, Chiba S (1978) Dynamic programming algorithm optimization for spoken word recognition. *IEEE Transactions on Acoustics, Speech, and Signal Processing* 26(1):43–49.

Schölkopf B, Platt JC, Shawe-Taylor J, Smola AJ, Williamson RC (2001) Estimating the support of a high-dimensional distribution. *Neural Computation* 13(7):1443–1471, URL <http://dx.doi.org/10.1162/089976601750264965>.

Schultz D, Jain BJ (2018) Nonsmooth analysis and subgradient methods for averaging in dynamic time warping spaces. *Pattern Recognition* 74:340–358.

Shi J, Malik J (2000) Normalized cuts and image segmentation. *IEEE Transactions on Pattern Analysis and Machine Intelligence* 22(8):888–905.

Song L, Huang J, Smola A, Fukumizu K (2009) Hilbert space embeddings of conditional distributions with applications to dynamical systems. *Proceedings of the 26th International Conference on Machine Learning (ICML)*.

Vlachos M, Kollios G, Gunopulos D (2002) Discovering similar multidimensional trajectories. *Proceedings of the 18th IEEE International Conference on Data Engineering (ICDE)*, 673–684.

Watson GS (1964) Smooth regression analysis. *Sankhyā: The Indian Journal of Statistics, Series A* 26(4):359–372.

Wenig P, Paparrizos J, Tsalouchidou I, Keogh E (2022) A comprehensive evaluation of time series anomaly detection algorithms. *Proceedings of the VLDB Endowment* 15(9):1779–1795, URL <http://dx.doi.org/10.14778/3538598.3538601>.

Yu S, Li H, Løkse S, Jenssen R, Príncipe JC (2023) The conditional cauchy–schwarz divergence with applications to time-series data and sequential decision making. *arXiv preprint arXiv:2301.08970* .

Yue Z, Wang Y, Duan J, Yang T, Huang C, Tong Y, Xu B (2022) Ts2vec: Towards universal representation of time series. *Proceedings of the AAAI Conference on Artificial Intelligence*.

Zhang Y, Petitjean F, Webb GI, Keogh E (2024) Distance-based time series clustering: Methods, benchmarks, and open problems. Available at: <https://arxiv.org/abs/2412.20582>.

Zhou T, Xu J, Pan W, Zhang C, Ding S, Chang Y (2021) Anomaly transformer: Time series anomaly detection with association discrepancy. *Advances in Neural Information Processing Systems (NeurIPS)*.